JVI Journals.ASM.org

Highly Specific Salt Bridges Govern Bacteriophage P22 Icosahedral Capsid Assembly: Identification of the Site in Coat Protein Responsible for Interaction with Scaffolding Protein

Juliana R. Cortines,[a]* Tina Motwani,[a] Aashay A. Vyas,[a] Carolyn M. Teschke[a,b]

Department of Molecular and Cell Biology,[a] and Department of Chemistry,[b] University of Connecticut, Storrs, Connecticut, USA

ABSTRACT

Icosahedral virus assembly requires a series of concerted and highly specific protein-protein interactions to produce a proper capsid. In bacteriophage P22, only coat protein (gp5) and scaffolding protein (gp8) are needed to assemble a procapsid-like particle, both *in vivo* and *in vitro*. In scaffolding protein's coat binding domain, residue R293 is required for procapsid assembly, while residue K296 is important but not essential. Here, we investigate the interaction of scaffolding protein with acidic residues in the N-arm of coat protein, since this interaction has been shown to be electrostatic. Through site-directed mutagenesis of genes 5 and 8, we show that changing coat protein N-arm residue 14 from aspartic acid to alanine causes a lethal phenotype. Coat protein residue D14 is shown by cross-linking to interact with scaffolding protein residue R293 and, thus, is intimately involved in proper procapsid assembly. To a lesser extent, coat protein N-arm residue E18 is also implicated in the interaction with scaffolding protein and is involved in capsid size determination, since a cysteine mutation at this site generated petite capsids. The final acidic residue in the N-arm that was tested, E15, is shown to only weakly interact with scaffolding protein's coat binding domain. This work supports growing evidence that surface charge density may be the driving force of virus capsid protein interactions.

IMPORTANCE

Bacteriophage P22 infects *Salmonella enterica* serovar Typhimurium and is a model for icosahedral viral capsid assembly. In this system, coat protein interacts with an internal scaffolding protein, triggering the assembly of an intermediate called a procapsid. Previously, we determined that there is a single amino acid in scaffolding protein required for P22 procapsid assembly, although others modulate affinity. Here, we identify partners in coat protein. We show experimentally that relatively weak interactions between coat and scaffolding proteins are capable of driving correctly shaped and sized procapsids and that the lack of these proper protein-protein interfaces leads to aberrant structures. The present work represents an important contribution supporting the hypothesis that virus capsid assembly is governed by seemingly simple interactions. The highly specific nature of the subunit interfaces suggests that these could be good targets for antivirals.

Viruses have a limited genome capacity, which results in a minimal number of distinct proteins used to build it. Icosahedral viral capsids are commonly formed by multiple copies of a single capsid protein (coat protein [CP]), organized as hexameric and pentameric capsomers. According to Caspar and Klug's icosahedral virus symmetry theory, coat proteins must adopt quasiequivalent conformations in order to generate a capsid (1). In addition, many double-stranded DNA (dsDNA) viruses, including herpesviruses, and the tailed bacteriophages T4, P2, λ, ϕ29, and P22 use auxiliary proteins to assist coat protein assembly (3). These proteins, often called scaffolding proteins (SPs), are necessary to initiate assembly and direct the correct morphology of viral capsids. In the case of bacteriophage P22, in the absence of scaffolding protein, coat protein gives rise to aberrant structures, including spirals, which result from a misplacement of pentons and a change in the curvature of the capsid subunits, and petite T=4 capsids (2, 4).

During its morphogenesis, P22's coat protein binds scaffolding protein in a nucleation-dependent reaction to form an intermediate structure called a procapsid (PC), which also has a portal protein complex and internal injection proteins (2, 5). DNA is then actively packaged through the unique portal protein channel, during which scaffolding protein exits through holes in the hexon capsomers and is recycled to generate new viral progeny (2). A morphological consequence of DNA packaging is capsid maturation, where the capsid expands by about 10% in diameter (6, 7).

Recently, two sets of subnanometer models based on cryo-electron microscopy data for P22's procapsid and mature capsid were reported (9, 12). From these studies, two similar models of the coat protein subunit were obtained for each state. Throughout this work, we discuss our findings based on the description of procapsid and mature subunit structures presented by Parent and colleagues (12). Five domains were defined: the N-arm (amino acids [aa] 1 to 56), E-loop (aa 57 to 82), P-domain (aa 83 to 143 and 346 to 420) with the P-loop (aa 376 to 398), A-domain (aa 144 to 222), and I-domain (insertion domain), previously called the

Received 6 January 2014 **Accepted** 25 February 2014

Published ahead of print 5 March 2014

Editor: L. Hutt-Fletcher

Address correspondence to Carolyn M. Teschke, teschke@uconn.edu.

* Present address: Juliana R. Cortines, Departamento de Virologia, Instituto de Microbiologia Paulo de Góes, Universidade Federal do Rio de Janeiro, Rio de Janeiro, Brazil.

doi:10.1128/JVI.00036-14

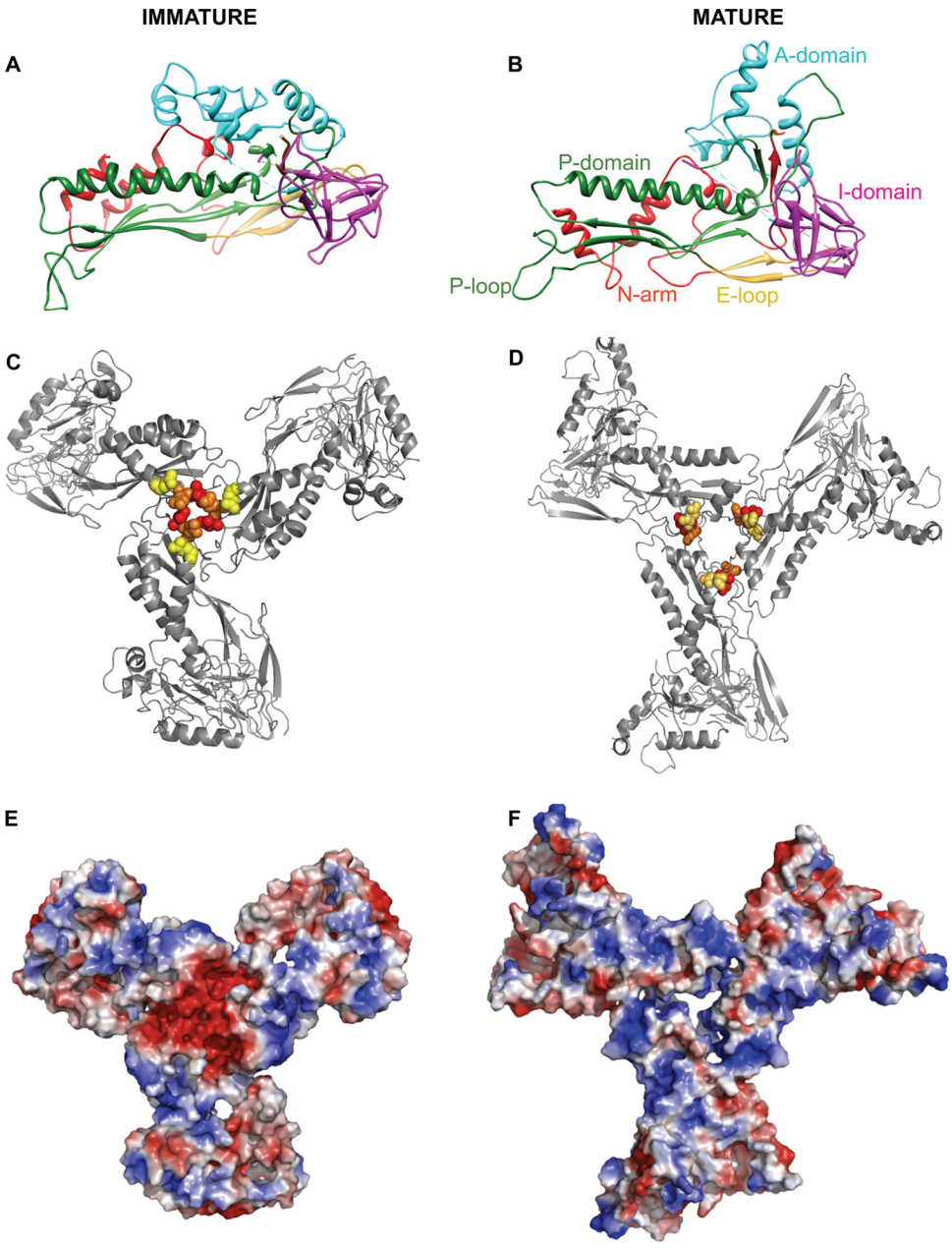

FIG 1 Models of phage P22 coat protein. (A) Procapsid (immature) coat protein monomer (PDB accession number 3IYI). (B) Expanded head (mature) coat protein monomer (PDB accession number 3IYH). For both models, N-arm is shown in red, E-loop is in yellow, P-domain is in green, A-domain is in cyan, and I-domain is in magenta. Domains are labeled accordingly. (C and D) Trimer tip region in procapsids (C) and expanded heads (D), viewed from the interior. Residues D14, E15, and E18 are represented as red, orange, and yellow spheres, respectively. (E and F) Surface charge densities from procapsids (E) and expanded heads (F), viewed from the interior. Figures were prepared by using PyMOL (PyMOL Molecular Graphics System, version 1.2r3pre; Schrödinger, LLC). Coat protein models are derived from a cryo-electron microscopy model reported previously (12).

telokin-like domain (aa 223 to 345). All domains are labeled and color coded in Fig. 1 (9, 10, 12). The N-arm region, in particular the two helices at the very N terminus, and the P-loop were implicated in capsid stability, as they participate in intersubunit interactions (9, 12). In addition, considerable conformational rearrangements of the N-arm, P-loop, and A-domain occur upon maturation (8, 10, 11), particularly at the location where three neighboring hexons meet in a region called "trimer tips," at the icosahedral 3-fold symmetry axis (4, 13). Evidence that scaffolding protein binds at the center of the true 3-fold and quasi-3-fold axes comes from difference mapping of cryo-electron microscopy densities for procapsids with and without scaffolding protein, where density was observed around the trimer tips in procapsids but not in expanded heads (4, 9, 13). The movement of the N-arm region during maturation, where scaffolding protein is thought to interact with coat protein, is striking, where charged residues, seen in a ball-and-stick representation in Fig. 1C and D, are rearranged spatially upon expansion (8). As a consequence, the surface

charges of this region drastically change from negative to positive upon maturation (Fig. 1E and F). In addition, there is also structural evidence suggesting that scaffolding protein may bind to the A-domain (9).

Scaffolding protein is 303 amino acids in length, organized mainly as α-helices; is extremely flexible; and exhibits an elongated shape (14–16). Coat protein binding occurs through scaffolding protein's C-terminal domain, at a helix-turn-helix motif (HTH) where about 30% of the residues are positively charged, indicating that the scaffolding protein-coat protein interaction is mostly electrostatic (17–19, 44). It exists in a monomer-dimer-tetramer equilibrium in solution, from which the dimer is the most active oligomer during PC nucleation (15). A minimum of 60 to 100 copies of scaffolding protein is needed, and a maximum of ~350 copies has been suggested to be present in PCs (9, 20, 21). A limited number of these are in direct contact with a high-affinity site on coat protein (the K_d [dissociation constant] of this interaction is in the nM range [15]), most likely arranged in an icosahedral fashion. However, the vast majority of scaffolding protein appears to be nonicosahedrally packed inside the procapsids and is probably the low-affinity binding population of scaffolding protein (9, 21–24).

Although extremely simple in its secondary structure, scaffolding protein adopts different conformations outside (in solution) and inside procapsids. In solution, the N-terminal and the C-terminal domains seem to be in close proximity, which is not true for the scaffolding protein population present inside procapsids (17, 25). Interestingly, the N-terminal domain of scaffolding protein, to a lesser extent, also affects the interaction of scaffolding protein and coat protein, possibly acting as a modulator to reduce the affinity between these two proteins (25–27). Recently, we determined the specific sites of interaction of scaffolding protein with coat protein. We found that scaffolding protein residues R293 and K296, both located in helix 2 of the HTH, are especially important. The arginine is crucial for scaffolding protein-coat protein interactions, whereas lysine 296 is a secondary binding site (26). The specific orientation of the HTH is also important for the proper interaction with coat protein (25). In the present study, we sought to identify, through site-directed mutagenesis and biochemical studies, the residues in coat protein involved in interactions with scaffolding protein and, therefore, procapsid assembly.

MATERIALS AND METHODS

Bacteria and phage stocks. Ampicillin-resistant plasmid pHBW-1 (28), coding for bacteriophage P22 coat protein (gene 5), was transformed into *Salmonella enterica* serovar Typhimurium strain DB7136 [*leuA414*(Am) *hisC525*(Am) *sup*^{0}] (29). Plasmid pET3a, coding for scaffolding protein (gene 8) and coat protein genes, was transformed into *Escherichia coli* BL21(DE3)/pLysS (30). The phage strains used in these studies carry an amber mutation in gene 5 (5$^-$ amber N114), which is Q173 to amber. The phage also carries the C1-7 mutation leading to a clear-plaque phenotype. Some phages also carried an amber mutation in gene 13 to prevent lysis.

Plasmids and mutations. Amino acid substitutions in coat protein were generated by site-directed mutagenesis in either plasmid pSE380 (Invitrogen, Carlsbad, CA) containing gene 5 (pHBW-1) (28) or pET3a containing gene 5 (coat protein) and gene 8 (scaffolding protein) ("assembler" plasmid, a gift from Peter E. Prevelige) by using the QuikChange protocol (Stratagene, Carlsbad, CA).

Efficiency of plating. The desired mutants were tested for their ability to produce viable phages. Plasmid pHBW-1 carrying the assorted mutations was transformed into *Salmonella* strain DB7136. A single colony of bacteria bearing a plasmid encoding each individual N-arm mutant was grown to mid-log phase, and cells were concentrated ~10-fold. Two drops of the cells were added to soft agar containing ampicillin at 100 μg/ml and IPTG (isopropyl β-D-1-thiogalactopyranoside) at 1 mM as well as enough 5$^-$ amber N114 phage to produce between 100 and 200 plaques/plate. Plates were incubated at different temperatures, ranging from 16°C to 41°C. The titer of phage complemented by coat protein expression from the plasmid was determined relative to the expression of wild-type (WT) coat protein, also expressed from the plasmid, at the permissive temperature (30°C). The results were plotted as a relative titer versus temperature. If the titer showed a decrease at low temperature (<30°C), the mutation was classified as promoting a cold-sensitive phenotype; if the decrease in titer was observed at a higher temperature (>30°C), the mutation was classified as promoting a temperature-sensitive phenotype. The same experiment was performed by using cells that overexpressed GroES/L from plasmid pGroESL (chloramphenicol resistant) (31) and transformed with pHBW-1 plasmids encoding WT coat protein and the E5A and D14A mutants.

***In vivo* phage production analysis.** Cultures of *Salmonella* DB7136 cells expressing either WT coat protein or N-arm coat variant proteins in plasmid pHBW-1 were grown to a density of 2×10^8 cells/ml in Luria-Bertani broth supplemented with 100 μg/ml ampicillin. The cells were then induced with 1 mM IPTG and infected with 5$^-$ 13$^-$ phage. After 10 min of infection, the phage-infected cells were split into three cultures, and each culture was incubated at different temperatures (30°C, 41°C, and 16°C). The 30°C and 41°C cultures were incubated for 3 h, whereas the 16°C culture was incubated for 6 h. After incubation, the cells were harvested and processed as previously described (32). Briefly, cells were lysed in the presence of 1 mM phenylmethylsulfonyl fluoride (PMSF) by freeze-thaw cycles. Cellular debris was separated from the soluble products. The supernatants were then centrifuged at >100,000 × *g* to precipitate assembled structures. The particles were suspended by shaking in a small volume of buffer and processed further, as described below.

Sucrose gradients. One hundred microliters of the suspended particles was applied to the top of a 5 to 20% (wt/wt) sucrose gradient, prepared by using a Gradient Master (model 106; Biocomp Instruments). Gradients were centrifuged at 104,813 × *g* for 35 min at 20°C in a Sorvall RC M120EX microultracentrifuge in an RP55S rotor. One-hundred-microliter fractions were collected from the top by using a positive-displacement Pipetteman. Samples were analyzed by 10% SDS-PAGE and electron microscopy.

Electron microscopy. Three microliters of assembly products of phage-infected cells was spotted onto carbon-coated copper grids. Samples were adsorbed for ~45 s, washed twice with water, and stained with 1% uranyl acetate. Grids were visualized by using a Fei Technai Biotwin instrument.

Expression of coat protein and scaffolding protein from a pET plasmid. Plasmid pET3a containing wild-type gene 5 and gene 8 (assembler plasmid) or these genes with mutations was transformed into BL21 cells. Cultures were grown to an optical density (OD) of 0.6 to 0.7, and expression was induced with 1 mM IPTG at 37°C. Cells were harvested by centrifugation at 15,000 × *g* for 15 min at 4°C. Supernatants were discarded, and cell pellets were resuspended in buffer B (50 mM Tris, 25 mM NaCl, 2 mM EDTA [pH 7.6]) and frozen at −20°C. Cells were thawed, and lysozyme (0.02%), DNase (50 μg/ml), RNase (50 μg/ml), and $MgCl_2$ (5 mM) were added. Following this, cells were sonicated (Misonix, Farmingdale, NY) on ice for 15 min, with the power set at 50%. Cellular debris was isolated by low-speed centrifugation (32,000 × *g* for 15 min in a Sorvall RC6+ superspeed centrifuge and an F18-12×50 rotor). Procapsids were then concentrated by centrifugation in a Sorvall Discover 90SE centrifuge using a T-865 rotor at 176,000 × *g* for 40 min at 4°C. Procapsid pellets were resuspended in buffer B overnight by shaking at 4°C. The impure procapsids were applied onto a ~100-ml Sepharose S1000 column with a flow rate of 0.2 ml/min in buffer B, and 4-ml fractions were collected. Fractions were analyzed by SDS-PAGE. The fractions with pure

procapsids were pooled, and the scaffolding protein was extracted as previously described (20). The resulting empty procapsid shells are called "shells" for simplicity.

Circular dichroism. The secondary structure of the N-arm coat variant proteins (D14A, E15A, and E18A) was analyzed by circular dichroism (CD) spectroscopy. Monomers of wild-type and N-arm coat variants were diluted to 0.2 mg/ml in 20 mM sodium phosphate buffer (pH 7.6). Spectra were measured with an Applied Photophysics instrument (Leatherhead, Surrey, United Kingdom) in a 1-mm-path-length cuvette maintained at 20°C. Wavelength scans were done at wavelengths between 195 and 250 nm with a 1-nm step, the band pass was set to 3 nm, and the time-per-point averaging was set to 55 s, leading to a scan time of ~51 min. The percent change in secondary structure was calculated by comparing the negative ellipticity of a mutant coat protein to that of the WT coat protein at 221 nm.

Assembly reactions. Coat protein shells were diluted 1:4 in 9 M urea for a final concentration of 2 mg/ml and incubated at room temperature for 30 min. The same volume of 20 mM sodium phosphate (pH 7.6) was added to the denatured shells, and the sample was extensively dialyzed against 20 mM sodium phosphate (pH 7.6). Coat monomers were centrifuged at >100,000 × *g* to separate monomers from any assembled coat protein. The monomer concentration was determined by the absorbance at 280 nm and using an extinction coefficient of 0.957. Assembly reactions were monitored by determining the increase in light scattering over time at 500 nm for 30 to 60 min. Coat monomers were rapidly mixed in a cuvette containing wild-type scaffolding protein, 20 mM sodium phosphate, and NaCl. Final concentrations were 0.5 mg/ml for coat protein and scaffolding protein and 60 mM for NaCl.

Immobilized scaffolding protein column. His-tagged wild-type scaffolding protein was loaded onto a cobalt-based affinity column to saturation (~5 mg/ml). One hundred microliters of the coat variant was then loaded onto the column at 0.2 mg/ml. The flow rate was 1.25 ml/min, and 0.25-ml fractions were collected. The fluorescence emission of the fractions was measured on a SLM Aminco Bowman 2 spectrofluorimeter with an excitation wavelength of 295 nm and an emission wavelength of 340 nm, with band passes of 1 and 8, respectively. Ovalbumin was used as a negative control, and WT coat protein was used as the positive control for binding to the scaffolding protein column. The ability of a coat protein variant to bind scaffolding protein was measured by comparing the elution times between the mutant protein and WT coat protein. Earlier elution times, similar to that of ovalbumin, are considered indicative of no or very weak interactions with scaffolding protein.

Cysteine mutant procapsid purification and analysis. We used pET3a coding for both wild-type coat and scaffolding genes as the template (a kind gift from Peter E. Prevelige). The desired mutations, as described below, were generated by using the QuikChange protocol (Stratagene, CA). Procapsids from the single mutants carrying cysteine substitutions in the N-arm domain of coat protein (D14C, E15C, and E18C) and double mutants carrying cysteine substitutions in both N-arm coat protein (CP) and scaffolding protein (SP) (CP-D14C/SP-R293C, CP-E15C/SP-R293C, CP-E18C/SP-R293C, CP-D14C/SP-K296C, CP-E15C/SP-K296C, and CP-E18C/SP-K296C) were generated. Procapsids carrying the individual substitutions were purified as described above. Samples were then loaded onto a ~10-ml Sepharose 4B column at a flow rate of 0.5 ml/min with buffer B as the elution buffer, and 0.75-ml fractions were collected and analyzed by SDS-PAGE. The fractions of interest were pooled, and purified procapsids were concentrated by high-speed centrifugation and resuspended in buffer B. The concentration of the pure procapsids was determined by using Pierce 660-nm protein assay reagent (Thermo Scientific, IL). Five micrograms of pure procapsids was separated under oxidizing (without β-mercaptoethanol) or reducing (with β-mercaptoethanol) conditions on 10% SDS-PAGE gels and run at 200 V. The gel was stained with Coomassie brilliant blue R-250. The bands corresponding to ~80 kDa present in the D14C/R293C, D14C/K296C, and E18C/K296C samples were cut and equilibrated in 500 μl of SDS reducing sample buffer (20 mM Tris-HCl [pH 7.6], 0.1% SDS, 20% glycerol, 1 mM EDTA, and 1.5 ml β-mercaptoethanol) and incubated at room temperature on a Nutator for 30 min. Following incubation, the gel strips were loaded onto a 10% SDS-PAGE gel.

RESULTS

Residues in the N-arm of coat protein are essential for scaffolding protein-coat protein interactions. Image reconstruction of procapsids suggests that scaffolding protein might interact with coat protein at the N-arm, the P-loop, and, potentially, the A-domain (4, 9, 12, 13). Here, we have probed the effect of amino acid substitutions in the N-arm and P-loop of coat protein on phage assembly. Interactions between the A-domain of coat protein and scaffolding protein will be the subject of a different study. Since we know that the critical residues in scaffolding protein are basic (R293 and K296), we concentrated our efforts on acidic residues in coat protein (17–19, 26). *Salmonella* strains transformed with plasmids that express coat protein with single substitutions in the N-arm (E5A, D14A, E15A, and E18A) or the P-loop (K377A and D385A) were infected with P22 phage carrying an amber mutation in gene 5 (codes for coat protein) and plated at different temperatures (Fig. 2A). If the synthesized coat protein can support growth of the gene 5 amber phage at each temperature, plaques would be observed. The efficiency of plating at each temperature was determined by comparison to the number of plaques when the WT coat protein was expressed from the plasmid at 30°C.

The P-loop region has an acidic patch in the procapsid at icosahedral 3-fold symmetry axes, so we reasoned that it might interact with the basic surface of the scaffolding protein HTH. To test the effect of charge changes in the P-loop on phage assembly, we mutated both basic and acidic amino acids. However, the K377A and D385A mutants displayed a wild-type phenotype by complementation, suggesting that this region is not involved in the interaction with scaffolding protein. Therefore, further experiments with these mutants were not performed.

In contrast, the coat protein N-arm mutants displayed either cold-sensitive or lethal phenotypes at 16°C by complementation (Fig. 2A). The lethal or cold-sensitive phenotypes became progressively less pronounced as the alanine substitution was moved further into the N-domain: E5A > D14 > E15 = E18. When E15A and E18A coat mutants were recombined into phage, they retained the cold-sensitive phenotype (data not shown), indicating that these substitutions cause defects in the context of the entire phage and not just when the gene is expressed from a plasmid, which can yield different protein levels compared to phage-expressed proteins. Interestingly, the E5A mutant resulted in a plating efficiency close to the reversion frequency of the gene 5-amber phage. The titer of the D14A mutant decreased by at least 3 orders of magnitude compared to the WT coat protein across the entire range of temperatures tested. These data suggest that the E5A and D14A mutants may each cause a lethal phenotype in complementation experiments. The growth of WT phage (no ambers) was unaffected by any of the plasmid-expressed mutant proteins at either 30°C or 16°C, indicating that even lethal mutations do not cause a dominant phenotype (data not shown). We next determined whether the coat protein substitutions E5A and D14A were lethal because of an inability of these mutants to bind scaffolding protein or because of a folding defect.

The E5A substitution in the N-arm affects coat protein folding. Although WT coat protein does not require chaperonins to

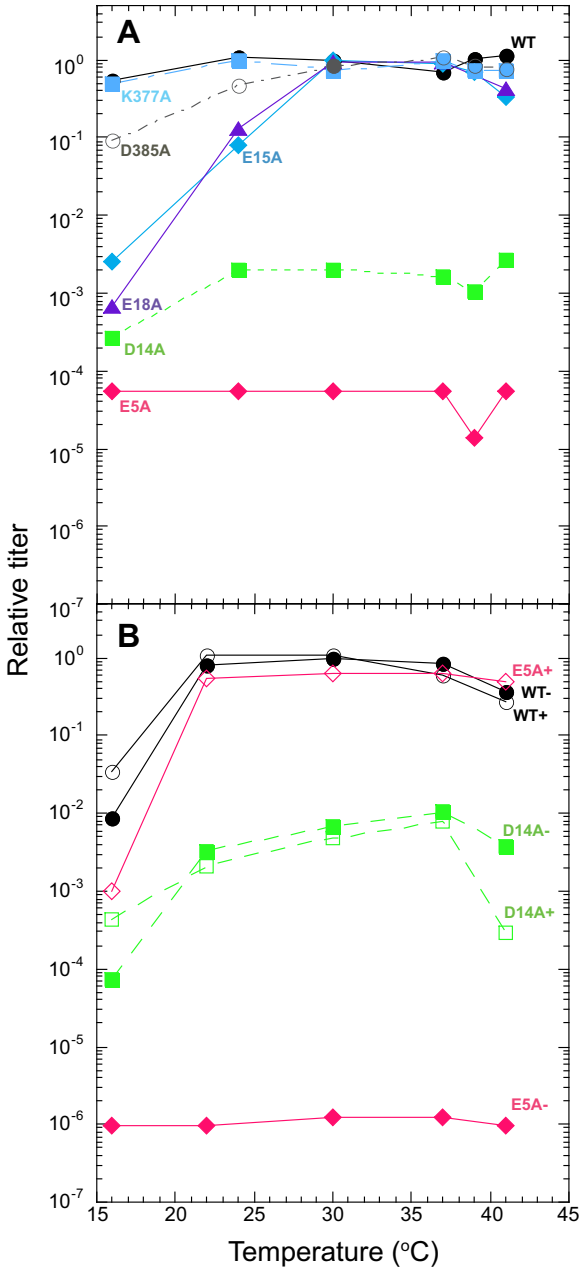

FIG 2 Effects of temperature and chaperones on phage growth of N-arm and P-domain coat protein mutants. The key for each mutant is included in the figure. (A) Efficiency of plating of the coat protein mutants. (B) Efficiency of plating in the presence or absence of GroES/L for coat protein E5A and D14A variants. Substitutions are indicated in the graphs; − or + signs represent the absence or presence of excess GroES/L, respectively. The reversion frequency of the 5^- amber phage was between 10^{-7} and 10^{-5}.

fold *in vivo*, temperature-sensitive-folding coat mutants can be rescued by overexpression of the GroES/L proteins resulting in viable progeny phage (33–35). If the E5A and D14A coat mutants cause a folding defect, coexpression of these mutants with extra GroES/L might rescue the assembly of infectious phages, and plating efficiencies would be expected to be similar to that of WT phage. The plasmid containing the E5A coat mutation was transformed into cells overexpressing GroES/L, and these cells were then infected with the gene 5 amber phage. Titers of the progeny were rescued to values similar to those of the WT coat protein, suggesting that the low values previously observed for the E5A mutant were due to misfolding and aggregation of coat protein (Fig. 2B). On the other hand, the poor titer of the coat protein D14A mutant was not affected by the overexpression of GroES/L. Thus, we conclude that the lethal phenotype of the D14A coat protein comes from the inability of the mutant coat protein to interact properly with scaffolding protein, rather than poor folding (Fig. 2B).

Less scaffolding protein is incorporated into procapsids assembled with N-arm mutant coat proteins. The morphological characteristics of the cold-sensitive N-arm coat protein mutants were determined in infected cells at 16°C. Here, cells producing the N-arm mutant proteins by expression from a plasmid were infected with phage that cannot generate coat protein or lyse the cells (gene 5^- amber and gene 13^- amber). The clarified lysates were applied onto sucrose gradients to observe the sedimentation of the assembly products. The gradient was fractionated, and the samples were run on SDS-polyacrylamide gels (Fig. 3A); fractions 16 and 22 were analyzed by electron microscopy to look for aberrant morphologies, which would be related to scaffolding protein interactions (Fig. 3B). A consistent deficiency in scaffolding protein incorporation in procapsids was observed, evidenced as a decrease in the intensity of the scaffolding protein band in the procapsid region (fractions 15 to 18) of the sucrose gradients. Also, a shift in the migration of the particles to a lower sucrose concentration (fractions 11 to 14) is consistent with a decrease in the amount of scaffolding protein within the particles. At this low temperature, the scaffolding protein interaction is apparently disfavored, and thus, aberrant structures are expected, as observed by the presence of spirals in all samples, except in fraction 16 of the gradient with wild-type procapsids. However, there is no evidence for petite particles in negative-stain electron micrographs, as shown by representative micrographs in Fig. 3B, or in fractions 11 to 14 for the E18A mutant (data not shown; see also below).

The data described above suggest that the N-arm of coat protein could be involved in interactions with scaffolding protein. In order to further investigate the effects of the D14A, E15A, and E18A substitutions in coat protein on interactions with scaffolding protein, we purified procapsids after coexpression of gene 8 (WT scaffolding protein) and gene 5 (carrying the individual N-arm mutations) from a pET plasmid. In our experience, more scaffolding protein is incorporated than usual when both WT proteins are expressed from this pET plasmid, so we can take advantage of this to compare levels of scaffolding protein when more protein than normal should be incorporated, thereby increasing the sensitivity of the assay by ~3-fold. When WT coat and scaffolding proteins are coexpressed, normal-sized assembled procapsids are the products of the preparation, with a coat protein-to-scaffolding protein ratio of ~0.6 (Fig. 4A, lane "WT"). Procapsids purified from phage-infected cells have a coat/scaffolding protein ratio of 1.4 to 2.0 (Fig. 4A, lane "2^- 13^-"). However, in the case of D14A coat protein, scaffolding protein could not be detected in the particles, suggesting that this coat mutant has a strong defect in scaffolding protein binding. The other mutants showed approximate coat/scaffolding protein ratios of 2.6 for E15A and 6.1 for E18A coat proteins, again indicating a smaller number of scaffolding proteins within the particles. The decreased amount of scaffolding protein detected in the procapsids made from alanine-

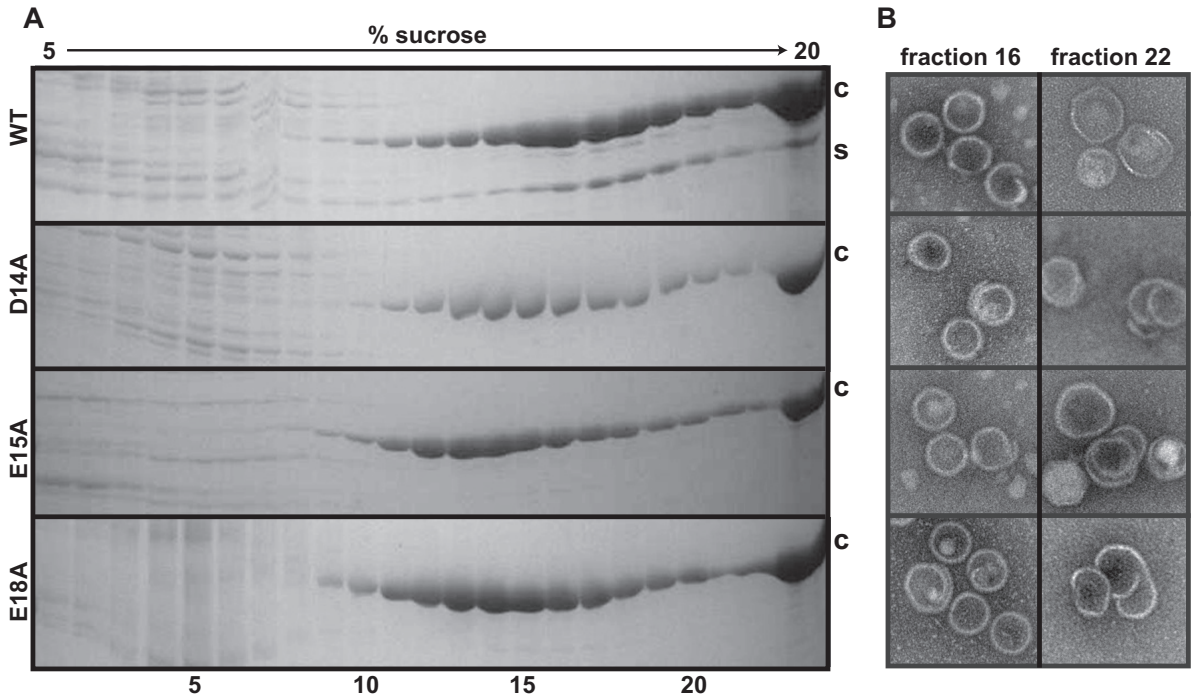

FIG 3 Procapsids generated from coat protein N-arm mutants have low or absent scaffolding protein incorporation at 16°C. (A) Analysis of protein profiles from a 5% (top) through 20% (bottom) sucrose gradient by 10% SDS-PAGE from cell lysates generated with WT and D14A, E15A, and E18A mutant coat proteins. Fractions are numbered at the bottom; positions of coat protein (c) and scaffolding protein (s) are indicated on the right. (B) Electron micrographs of the corresponding sucrose gradients (shown on the left). Fractions 16 and 22 usually correspond to procapsids and phage or aberrant morphologies, respectively.

substituted coat protein mutants is not a consequence of scaffolding protein expression, as equivalent amounts of this protein are expressed from each plasmid (data not shown). Based on these results, we hypothesize that residues D14, E15, and E18 are part of the coat protein-scaffolding protein interaction interface, with D14 being the principal interaction site between the two proteins.

One possible explanation for the decrease in the binding of scaffolding protein by D14A coat protein is that the substitution affects the folding of coat protein in a way that cannot be rescued by GroES/L (Fig. 2B). Refolded cold-sensitive T10I and R101C coat proteins have altered secondary structures compared to the wild-type coat protein, as monitored by circular dichroism spectra, showing decreases in negative ellipticity at 221 nm of 35 and 42%, respectively (36). However, all of the N-arm mutants (D14A, E15A, or E18A) showed CD spectra reasonably similar to those of the WT protein (Fig. 5A). The D14A mutant showed the greatest change, with a decrease in negative ellipticity at 221 nm of only about 17%. Therefore, the decrease in scaffolding binding is not likely a result of secondary structure changes. In addition, *in vitro* assembly reactions of the N-arm coat protein mutants showed that none of them are capable of supporting assembly (Fig. 5B). Since all the proteins have similar secondary structures, the inability to assemble or to bind scaffolding protein *in vitro* is caused by local changes in the N-arm and not the overall structure.

All of the N-arm mutants can interact somewhat with scaffolding protein *in vivo*, since WT-like procapsids were observed (Fig. 4) when coat and scaffolding proteins were coexpressed. In addition, the E15A and E18A coat variants can support phage growth at a permissive temperature (Fig. 2), which means that some scaffolding protein must participate in assembly, as it is required for the incorporation of essential minor proteins into procapsids. One way to determine the relative affinity of the N-arm coat protein mutants is to immobilize His-tagged scaffolding protein onto a metal affinity column and use this as a weak-affinity matrix. Through this method, weak affinity between coat and scaffolding proteins can be qualitatively observed (32, 37, 38). If the N-arm coat protein mutant monomers interact with scaffolding protein, a delay in elution is expected. Ovalbumin is used as a negative control, since it does not bind to coat protein (32). Fluorescence emission of the fractions from the scaffolding protein affinity matrix was measured to determine the volume needed to elute each protein (Fig. 5C). Ovalbumin and all the N-arm mutants eluted at 1.5 ml, whereas WT coat protein eluted at 2.25 ml. This observation leads to the conclusion that the mutant coat proteins are deficient in scaffolding protein binding. However, as mentioned above, heterologous expression of genes 5 and 8 was able to generate significant levels of wild-type-like procapsids, supporting the conclusion that, even though very deficient for scaffolding protein binding, the N-arm mutants remain assembly competent, at least enough to initiate nucleation and support the elongation reaction to assemble procapsids *in vivo*. Another possibility is that a cellular or viral factor not present in the *in vitro* reaction, like chaperones or DNA, may promote procapsid assembly.

Residue D14 of coat protein is in close contact with residue R293 of scaffolding protein. Previous results from our laboratory showed that arginine 293 and lysine 296 at the C-terminal HTH domain of scaffolding protein are crucial for interactions with coat protein and for supporting procapsid assembly (26). If positions D14, E15, and E18 in coat protein are potential sites for

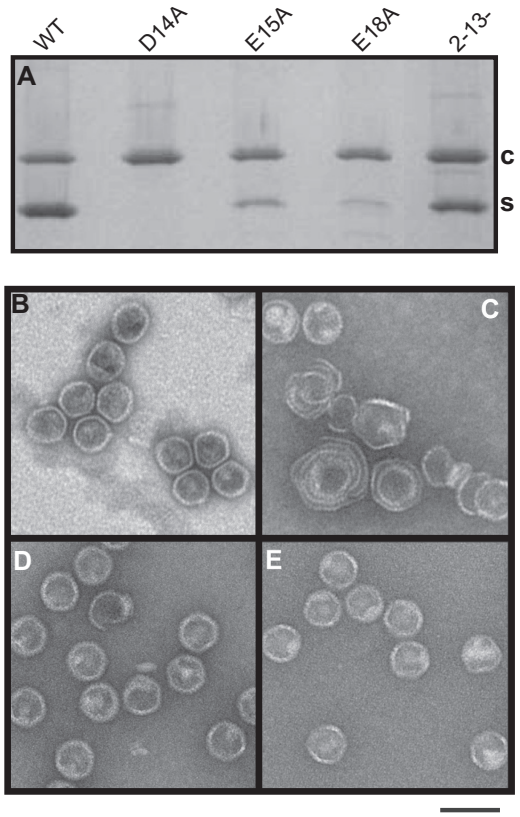

FIG 4 The coat protein D14A mutant is highly defective in scaffolding protein binding. (A) Purified procapsids with the D14A, E15A, or E18A coat protein run on 10% SDS-PAGE gels to analyze protein content. WT procapsids generated from coexpression of coat and scaffolding proteins from the pET3a plasmid and WT procapsids from 2^- 13^- phage-infected cells are shown as controls. The migration of coat protein is indicated by "c," and the migration of scaffolding protein is indicated by "s." (B to E) Electron micrographs of particles generated from WT (B) and D14A (C), E15A (D), and E18A (E) coat proteins, showing significantly aberrant structures for the D14A mutant but not for the other mutants. The bar represents 100 nm.

interactions with scaffolding protein, they should be in close proximity to SP-R293 or SP-K296 (note that from this point on, when referring to specific mutant proteins, we designate them SP for scaffolding protein or CP for coat protein, followed by the amino acid residue that has been mutated and the residue to which it was changed). We tested this hypothesis by generating a cysteine mutant at each of these coat protein sites in conjunction with SP-R293C or SP-K296C. We made expression plasmids carrying the CP-D14C/SP-R293C, CP-E15C/SP-R293C, CP-E18C/SP-R293C, CP-D14C/SP-K296C, CP-E15C/SP-K296C, and CP-E18C/SP-K296C double mutants. Procapsids of all six double mutants were purified under oxidizing conditions, and the products were analyzed by nonreducing SDS-PAGE. The D14C, E15C, and E18C single coat protein mutants were also purified as controls for disulfide bond formation and scaffolding protein content. A thick band at ~80 kDa was observed mainly for the CP-D14C/SP-R293C double mutant, with less pronounced bands at the same position for the CP-E15C/SP-R293C, CP-E18C/SP-R293C, CP-D14C/SP-K296C, and CP-E18C/SP-K296C mutants (Fig. 6). The highest-intensity bands running at ~80 kDa (CP-D14C/SP-R293C, CP-D14C/SP-K296C, and CP-E18C/SP-K296C) were excised from the gel and reapplied onto a reducing SDS-PAGE gel, confirming the presence of the mutant coat and scaffolding proteins in the bands (Fig. 6B). The distance of a disulfide bond is about 6 Å, indicating that coat protein amino acids, especially residue 14 of coat protein, and scaffolding protein residue 293 are in very close proximity in procapsids. The substitution at D14 causes the most pronounced effect on procapsid morphology, as observed by the higher percentage of aberrant structures in the electron micrographs of the purified procapsids (Fig. 4C).

As measured by densitometry of the gel bands, CP-D14C/SP-R293C generated approximately 14 or 6 times more disulfide-bonded coat protein-scaffolding protein complex than did CP-E15C/SP-R293C or CP-E18C/SP-R293C, respectively, suggesting that the interaction is preferentially formed by CP-D14C and SP-R293C. In addition, CP-E18C marginally favored interactions with SP-K296C, having about 2-fold more disulfide CP-SP complex than CP-D18C/SP-R293C, an indication of a weaker secondary site of interaction. Position E15 in the coat protein N-arm appears to be the most ineffective at interactions with scaffolding protein. An interesting observation is that substitution of the glutamic acid at position 18 for cysteine resulted in the formation of petite procapsids (Fig. 6C to E). These result from a change in the curvature of capsid subunits, in which the triangulation number is T=4. To date, only substitutions in the I-domain have resulted in petite capsids (27), so a new site for size determination has been identified.

DISCUSSION

A few highly specific salt bridges govern bacteriophage P22 procapsid assembly. In the C-terminal domain of scaffolding protein, the arginine at position 293 is the primary amino acid residue responsible for supporting procapsid formation. A secondary player, lysine 296, is important but not essential for assembly (26). We found that one amino acid in coat protein was critical for interactions with scaffolding protein: D14. Residues E15 and E18 were also shown to be involved but did not lead to a lethal phenotype in complementation experiments. We cannot rule out the possibility that substitution of an aspartic acid by an alanine may disrupt the N-arm helix disposition/structure at the trimer tip. However, we do not believe that this is likely to happen, since alanine has a high helical propensity. Another possibility is that the mutation of Asp to Ala may have affected the charge distribution of the scaffolding protein interaction site in coat protein, thus drastically affecting the coat protein-scaffolding protein interaction. However, overall surface charge calculations suggest that it was not substantially changed due to the mutation (not shown).

To confirm the specific interaction between coat and scaffolding proteins, double cysteine mutants were generated with one cysteine in the N-arm of coat protein and another cysteine at position R293 or K296 of the coat-binding HTH of scaffolding protein. It is evident that, from all possibilities tested, coat protein residue D14 and scaffolding protein residue R293 form the closest interaction, showing the largest amount of the disulfide-bonded coat protein-scaffolding protein heterooligomer compared to all other pairs (Fig. 6). Residues D14 and E18 in coat protein also bind scaffolding protein residue K296. In this case, coat protein residue E18 shows a marginal preference for scaffolding protein residue K296 compared to that of coat protein residue D14. When residue E15 is mutated to cysteine, it is able to make a small amount of disulfide with the scaffolding protein R293C mutation.

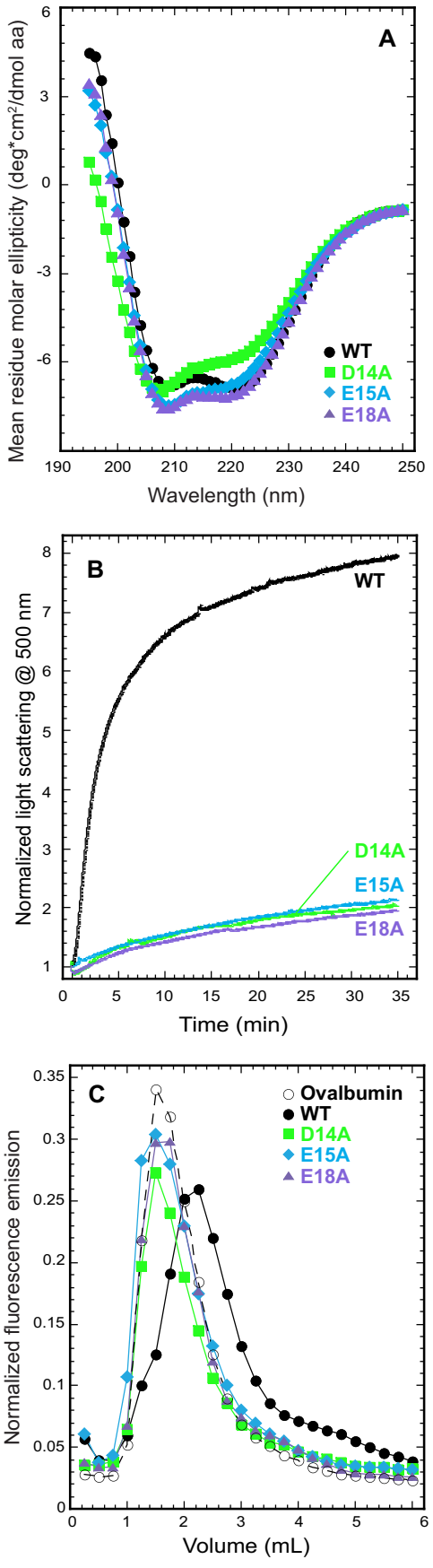

Although there is clearly a strong preference for the interaction with coat protein residue D14, scaffolding protein shows some promiscuity when it comes to the site of interaction. Since the coat mutants are in a loop between two helices of the N-arm, this small amount of variation in binding could be expected, especially since it is not arranged in a strict icosahedral fashion. Our data additionally suggest that the N-arm of coat protein is the primary site for interactions with scaffolding protein that are required for procapsid assembly. This confirms previous cryo-electron microscopy data that showed densities at the trimer tip area on procapsids but not in expanded heads (4). Changing the essential coat protein residue D14 leads to a lethal phenotype for phage production and aberrant structures even when expressed from a plasmid, which produces more scaffolding protein than wild-type procapsids produced by 2^{-} 13^{-} phage-infected cells. Interaction with the A-domain, as suggested previously (9), may still occur and may be important for direction assembly of the properly sized capsid.

Our working hypothesis for the nucleation of bacteriophage P22 assembly is that charged residues in the N-arm of coat protein are closely placed in space to form a negative patch to which the positively charged HTH domain of scaffolding protein is attracted. The scaffolding protein HTH domain binds preferentially to coat protein residue D14, which we suggest forms the high-affinity site. The evident opposite-charged patches on P22's coat protein and scaffolding protein (Fig. 1) attract both proteins toward each other, to make possible the formation of the nuclei that will be the basis for procapsid assembly. Scaffolding protein possibly acts as the charged nucleator (much like nucleic acids behave in other systems, as mentioned above), to which coat protein arranges around via coulombic interactions. During maturation, the charges on the coat protein inner surface are rearranged such that the surface becomes positive, in a mechanism similar to that of bacteriophage HK97 (39). The scaffolding protein is then repelled from its interaction with coat protein and escapes through holes in the lattice. This now positively charged surface can interact with DNA during packaging. Thus, the surface charge density has been shown to be very important, where, in the case of viral capsids, the total charges of protein subunits are the fundamental forces that drive size determination and proper core assembly (40).

Conformational switching and size determination are multilocus features. We also observed that the coat protein E18C mutant, but not the E18A mutant, has the tendency to form petite procapsids. To generate a T=4 capsid, the curvature of coat protein must increase. Thus, the cysteine at this position is forcing a change in the curvature of the capsomers. From the data presented here, we conclude that different regions in coat protein control

FIG 5 Inability of the N-arm coat protein mutants to form procapsids or bind scaffolding protein *in vitro* is not due to secondary-structure changes. (A) Secondary structure of WT, D14A, E15A, and E18A coat protein monomers assessed by circular dichroism spectroscopy. (B) Monomers of the N-arm D14A, E15A, and E18A mutants were produced, and assembly was caused by addition of scaffolding protein. The assembly reactions were monitored by light scattering at 500 nm. Assembly of the WT coat protein with scaffolding protein is shown for comparison. (C) Scaffolding protein was immobilized on a metal affinity matrix, and the elution profile of mutant and WT coat proteins is shown. The fluorescence emission of each fraction was measured and plotted as a function of time. Ovalbumin was used as a negative control. In all panels, the key to the symbols is shown.

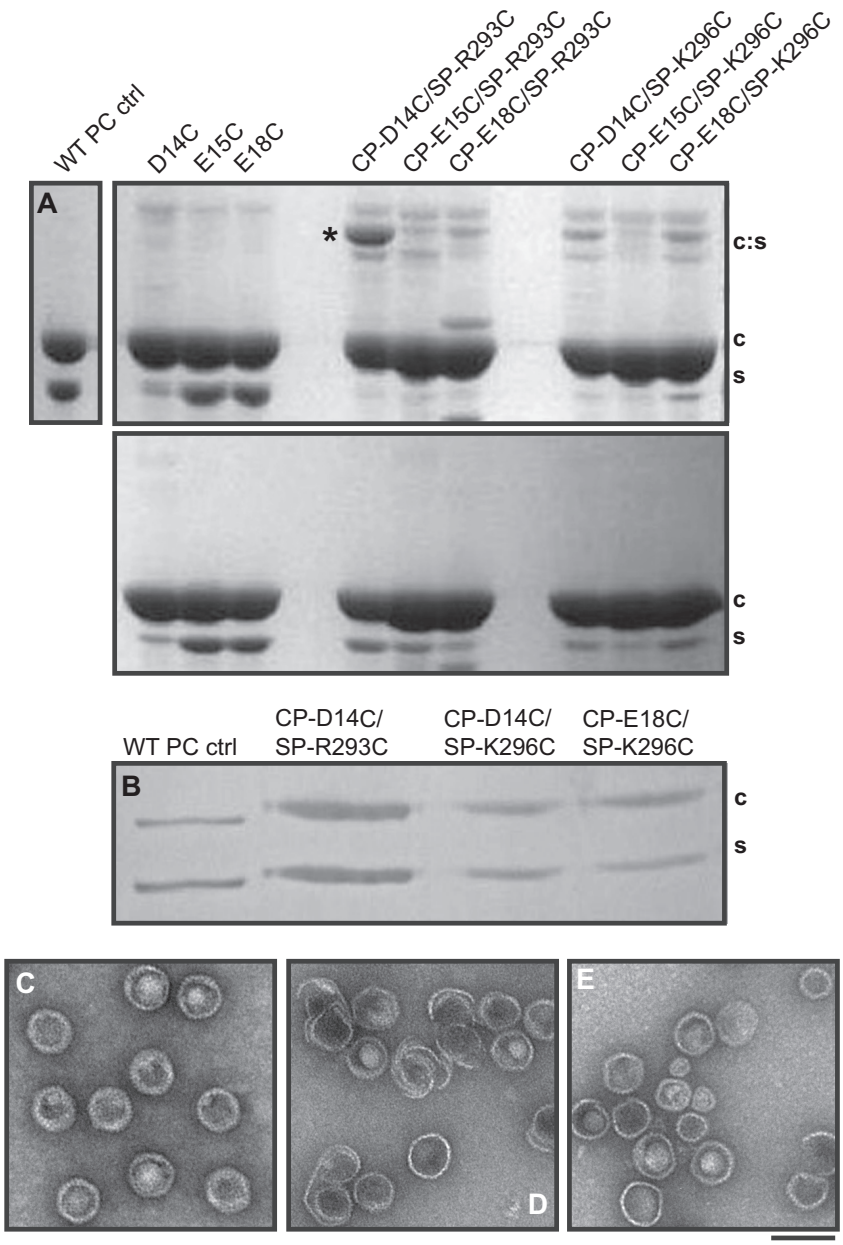

FIG 6 The coat protein D14C mutant binds strongly to the scaffolding protein R293C mutant and not to other N-arm residues in procapsids. (A) SDS-PAGE analysis of procapsids of CP-D14C, CP-E15C, CP-E18C, CP-D14C/SP-R293C, CP-E15C/SP-R293C, CP-E18C/SP-R293C, CP-D14C/SP-K296C, CP-E15C/SP-K296C, and CP-E18C/SP-K296C cysteine mutants. An intense band at ~80 kDa was observed for the CP-D14C/SP-R293C double mutant, indicated by the asterisk. This band was not as pronounced for any of the other five double-cysteine mutants. (B) Two-dimensional reducing SDS-PAGE gel for the CP-D14C/SP-R293C, CP-D14C/SP-K296C, and CP-E18C/SP-K296C ~80-kDa bands. (C to E) Electron micrographs of negatively stained CP-D14C/SP-R293C (C), CP-E15C/SP-R293C (D), and CP-E18C/SP-R293C (E) particles. The bar represents 100 nm.

size determination. The first important site is residue A285, located at the I-domain (27). We hypothesize that both variants actually affect the conformation of the A-domain. The A-domain must be flexible to achieve the proper curvature, and we have shown that mutants that affect size determination also affect flexibility of the A-domain (32). Changing the conformation of the N-arm may affect interactions with the spine helix and, consequently, the A-domain. It is intriguing that changing residue E5 to an alanine affected the ability of the entire protein to fold properly, suggesting that the very amino-terminal helix must interact with another region of the protein to promote folding.

Comparison with other scaffolding-dependent systems. In this work, we show that in phage P22, coat protein and scaffolding protein have very specific interaction sites that direct robust assembly mainly through two amino acids. There are both similarities and differences between phage P22 and other dsDNA viruses having a genetically distinct scaffolding protein in the understanding of interactions between coat and scaffolding proteins. For example, in bacteriophage phi29, a disordered region at the C terminus of its scaffolding protein (residues 79 to 97) appears to interact with capsid protein (41, 42). This amino-terminal HTH domain is important for folding but not assembly (41). Interest-

ingly, phi29's and P22's scaffolding proteins have similar folds, with the secondary structure being predominantly α-helical. The N-terminal region of phi29 scaffolding protein can be superimposed nicely onto P22's C terminus. However, as noted above, the termini from both proteins have opposite coat protein interaction functions (43). Although the specific sites of interaction between capsid and scaffolding proteins in phi29 are not established, the interaction is likely to involve electrostatic interactions (41). Although much less well characterized, another example is the eukaryotic alphaherpesviruses, where it appears that the C-terminal region of the UL26.5 scaffolding protein (amino acids 622 to 633) is important for procapsid assembly (45, 46). The interaction with the VP5 capsid protein is through hydrophobic interactions, unlike P22 (47). In a second-site suppressor search of scaffolding mutants that no longer interact with VP5, 65% of the suppressors were found in two proposed helices at the amino terminus of VP5 capsid protein (48), which is surprisingly similar to that seen in P22, although this certainly could be a coincidence. As a final example, single-stranded DNA bacteriophage phiX174 also uses an internal scaffolding protein, as well as an external scaffolding protein, to build its procapsid (42). Again, the C termini are involved in coat protein interactions: aromatic residues in this region form the scaffolding protein-coat protein interaction interface (49, 50). In addition to the aromatics, two acidic residues in scaffolding protein make salt bridges with basic residues in coat protein and are also implicated in assembly (51). Regardless of the exact details, it is clear that viruses have developed extremely simple yet elegant ways of controlling the interaction between their protein building blocks to regulate a finely tuned process leading to capsid assembly.

ACKNOWLEDGMENTS

This work was supported by National Institutes of Health grant GM076661 to C.M.T.

We thank Margaret Suhanovsky for instructive discussions throughout manuscript preparation and Marie Cantino and Steve Daniels from the University of Connecticut Electron Microscopy Center for technical guidance on the electron microscopy experiments.

REFERENCES

1. **Caspar DLD, Klug A.** 1962. Physical principles in the construction of regular viruses. Cold Spring Harb. Symp. Quant. Biol. **27:**1–24. http://dx.doi.org/10.1101/SQB.1962.027.001.005.
2. **King J, Casjens S.** 1974. Catalytic head assembly protein in virus morphogenesis. Nature **251:**112–119. http://dx.doi.org/10.1038/251112a0.
3. **Dokland T, Bernal RA, Burch A, Pletnev S, Fane BA, Rossmann MG.** 1999. The role of scaffolding proteins in the assembly of the small, single-stranded DNA virus phiX174. J. Mol. Biol. **288:**595–608. http://dx.doi.org/10.1006/jmbi.1999.2699.
4. **Thuman-Commike PA, Greene B, Malinski JA, Burbea M, McGough A, Chiu W, Prevelige PE, Jr.** 1999. Mechanism of scaffolding-directed virus assembly suggested by comparison of scaffolding-containing and scaffolding-lacking P22 procapsids. Biophys. J. **76:**3267–3277. http://dx.doi.org/10.1016/S0006-3495(99)77479-5.
5. **Botstein D, Waddell CH, King J.** 1973. Mechanism of head assembly and DNA encapsulation in *Salmonella* phage P22. I. Genes, proteins, structures and DNA maturation. J. Mol. Biol. **80:**669–695.
6. **Prasad BVV, Prevelige PE, Jr, Marieta E, Chen RO, Thomas D, King J, Chiu W.** 1993. Three-dimensional transformation of capsids associated with genome packaging in a bacterial virus. J. Mol. Biol. **231:**65–74. http://dx.doi.org/10.1006/jmbi.1993.1257.
7. **Earnshaw W, Casjens S, Harrison SC.** 1976. Assembly of the head of bacteriophage P22: X-ray diffraction from heads, proheads and related structures. J. Mol. Biol. **104:**387–410. http://dx.doi.org/10.1016/0022-2836(76)90278-3.
8. **Parent KN, Sinkovits RS, Suhanovsky MM, Teschke CM, Egelman EH, Baker TS.** 2010. Cryo-reconstructions of P22 polyheads suggest that phage assembly is nucleated by trimeric interactions among coat proteins. Phys. Biol. **7:**045004. http://dx.doi.org/10.1088/1478-3975/7/4/045004.
9. **Chen DH, Baker ML, Hryc CF, Dimaio F, Jakana J, Wu W, Dougherty M, Haase-Pettingell C, Schmid MF, Jiang W, Baker D, King JA, Chiu W.** 2011. Structural basis for scaffolding-mediated assembly and maturation of a dsDNA virus. Proc. Natl. Acad. Sci. U. S. A. **108:**1355–1360. http://dx.doi.org/10.1073/pnas.1015739108.
10. **Teschke CM, Parent KN.** 2010. 'Let the phage do the work': using the phage P22 coat protein structures as a framework to understand its folding and assembly mutants. Virology **401:**119–130. http://dx.doi.org/10.1016/j.virol.2010.02.017.
11. **Kang S, Prevelige PE, Jr.** 2005. Domain study of bacteriophage p22 coat protein and characterization of the capsid lattice transformation by hydrogen/deuterium exchange. J. Mol. Biol. **347:**935–948. http://dx.doi.org/10.1016/j.jmb.2005.02.021.
12. **Parent KN, Khayat R, Tu LH, Suhanovsky MM, Cortines JR, Teschke CM, Johnson JE, Baker TS.** 2010. P22 coat protein structures reveal a novel mechanism for capsid maturation: stability without auxiliary proteins or chemical crosslinks. Structure **18:**390–401. http://dx.doi.org/10.1016/j.str.2009.12.014.
13. **Thuman-Commike PA, Greene B, Jakana J, McGough A, Prevelige PE, Jr, Chiu W.** 2000. Identification of additional coat-scaffolding interactions in a bacteriophage P22 mutant defective in maturation. J. Virol. **74:**3871–3873. http://dx.doi.org/10.1128/JVI.74.8.3871-3873.2000.
14. **Tuma R, Parker MH, Weigele P, Sampson L, Sun Y, Krishna NR, Casjens S, Thomas GJ, Jr, Prevelige PE, Jr.** 1998. A helical coat protein recognition domain of the bacteriophage P22 scaffolding protein. J. Mol. Biol. **281:**81–94. http://dx.doi.org/10.1006/jmbi.1998.1916.
15. **Parker MH, Stafford WF, III, Prevelige PE, Jr.** 1997. Bacteriophage P22 scaffolding protein forms oligomers in solution. J. Mol. Biol. **268:**655–665. http://dx.doi.org/10.1006/jmbi.1997.0995.
16. **Sun Y, Parker MH, Weigele P, Casjens S, Prevelige PE, Jr, Krishna NR.** 2000. Structure of the coat protein-binding domain of the scaffolding protein from a double-stranded DNA virus. J. Mol. Biol. **297:**1195–1202. http://dx.doi.org/10.1006/jmbi.2000.3620.
17. **Parker MH, Casjens S, Prevelige PE, Jr.** 1998. Functional domains of bacteriophage P22 scaffolding protein. J. Mol. Biol. **281:**69–71. http://dx.doi.org/10.1006/jmbi.1998.1917.
18. **Weigele PR, Sampson L, Winn-Stapley DA, Casjens SR.** 2005. Molecular genetics of bacteriophage P22 scaffolding protein's functional domains. J. Mol. Biol. **348:**831–844. http://dx.doi.org/10.1016/j.jmb.2005.03.004.
19. **Parent KN, Doyle SM, Anderson E, Teschke CM.** 2005. Electrostatic interactions govern both nucleation and elongation during phage P22 procapsid assembly. Virology **340:**33–45. http://dx.doi.org/10.1016/j.virol.2005.06.018.
20. **Prevelige PE, Jr, Thomas D, King J.** 1988. Scaffolding protein regulates the polymerization of P22 coat subunits into icosahedral shells *in vitro*. J. Mol. Biol. **202:**743–757. http://dx.doi.org/10.1016/0022-2836(88)90555-4.
21. **Parker MH, Brouillette CG, Prevelige PE, Jr.** 2001. Kinetic and calorimetric evidence for two distinct scaffolding protein binding populations within the bacteriophage P22 procapsid. Biochemistry **40:**8962–8970. http://dx.doi.org/10.1021/bi0026167.
22. **Teschke CM, King J, Prevelige PE, Jr.** 1993. Inhibition of viral capsid assembly by 1,1'-bi(4-anilinonaphthalene-5-sulfonic acid). Biochemistry **32:**10658–10665.
23. **Greene B, King J.** 1994. Binding of scaffolding subunits within the P22 procapsid lattice. Virology **205:**188–197. http://dx.doi.org/10.1006/viro.1994.1634.
24. **Thuman-Commike PA, Greene B, Jokana J, Prasad BVV, King J, Prevelige PE, Jr, Chiu W.** 1996. Three-dimensional structure of scaffolding-containing phage P22 procapsids by electron cryo-microscopy. J. Mol. Biol. **260:**85–98. http://dx.doi.org/10.1006/jmbi.1996.0383.
25. **Padilla-Meier GP, Teschke CM.** 2011. Conformational changes in bacteriophage p22 scaffolding protein induced by interaction with coat protein. J. Mol. Biol. **410:**226–240. http://dx.doi.org/10.1016/j.jmb.2011.05.006.
26. **Cortines JR, Weigele PR, Gilcrease EB, Casjens SR, Teschke CM.** 2011. Decoding bacteriophage P22 assembly: identification of two charged residues in scaffolding protein responsible for coat protein interaction. Virology **421:**1–11. http://dx.doi.org/10.1016/j.virol.2011.09.005.
27. **Suhanovsky MM, Teschke CM.** 2011. Bacteriophage P22 capsid size determination: roles for the coat protein telokin-like domain and the scaf-

folding protein amino-terminus. Virology **417:**418–429. http://dx.doi.org/10.1016/j.virol.2011.06.025.
28. **Parent KN, Suhanovsky MM, Teschke CM.** 2007. Polyhead formation in phage P22 pinpoints a region in coat protein required for conformational switching. Mol. Microbiol. **65:**1300–1310. http://dx.doi.org/10.1111/j.1365-2958.2007.05868.x.
29. **Winston R, Botstein D, Miller JH.** 1979. Characterization of amber and ochre suppressors in *Salmonella typhimurium*. J. Bacteriol. **137:**433–439.
30. **Studier FW, Rosenberg AH, Dunn JJ, Dubendorff JW.** 1990. Use of T7 RNA polymerase to direct expression of cloned genes. Methods Enzymol. **185:**60–89. http://dx.doi.org/10.1016/0076-6879(90)85008-C.
31. **Goloubinoff P, Gatenby AA, Lorimer GH.** 1989. GroE heat-shock proteins promote assembly of foreign prokaryotic ribulose bisphosphate carboxylase oligomers in Escherichia coli. Nature **337:**44–47. http://dx.doi.org/10.1038/337044a0.
32. **Suhanovsky MM, Parent KN, Dunn SE, Baker TS, Teschke CM.** 2010. Determinants of bacteriophage P22 polyhead formation: the role of coat protein flexibility in conformational switching. Mol. Microbiol. **77:**1568–1582. http://dx.doi.org/10.1111/j.1365-2958.2010.07311.x.
33. **Gordon CL, Sather SK, Casjens S, King J.** 1994. Selective *in vivo* rescue by GroEL/ES of thermolabile folding intermediates to phage P22 structural proteins. J. Biol. Chem. **269:**27941–27951.
34. **Nakonechny WS, Teschke CM.** 1998. GroEL and GroES control of substrate flux in the *in vivo* folding pathway of phage P22 coat protein. J. Biol. Chem. **273:**27236–27244. http://dx.doi.org/10.1074/jbc.273.42.27236.
35. **Parent KN, Teschke CM.** 2007. GroEL/S substrate specificity based on substrate unfolding propensity. Cell Stress Chaperones **12:**20–32. http://dx.doi.org/10.1379/CSC-219R.1.
36. **Fong DG, Doyle SM, Teschke CM.** 1997. The folded conformation of phage P22 coat protein is affected by amino acid substitutions that lead to a cold-sensitive phenotype. Biochemistry **36:**3971–3980. http://dx.doi.org/10.1021/bi962188y.
37. **Zopf D, Ohlson S.** 1990. Weak-affinity chromatography. Nature **346:**87–88. http://dx.doi.org/10.1038/346087a0.
38. **Teschke CM, Fong DG.** 1996. Interactions between coat and scaffolding proteins of phage P22 are altered *in vitro* by amino acid substitutions in coat protein that cause a cold-sensitive phenotype. Biochemistry **35:**14831–14840. http://dx.doi.org/10.1021/bi960860l.
39. **Conway JF, Wikoff WR, Cheng N, Duda RL, Hendrix RW, Johnson JE, Steven AC.** 2001. Virus maturation involving large subunit rotations and local refolding. Science **292:**744–748. http://dx.doi.org/10.1126/science.1058069.
40. **Daniel MC, Tsvetkova IB, Quinkert ZT, Murali A, De M, Rotello VM, Kao CC, Dragnea B.** 2010. Role of surface charge density in nanoparticle-templated assembly of bromovirus protein cages. ACS Nano **4:**3853–3860. http://dx.doi.org/10.1021/nn1005073.
41. **Fu CY, Morais MC, Battisti AJ, Rossmann MG, Prevelige PE, Jr.** 2007. Molecular dissection of phi29 scaffolding protein function in an in vitro assembly system. J. Mol. Biol. **366:**1161–1173. http://dx.doi.org/10.1016/j.jmb.2006.11.091.
42. **Prevelige PE, Fane BA.** 2012. Building the machines: scaffolding protein functions during bacteriophage morphogenesis. Adv. Exp. Med. Biol. **726:**325–350. http://dx.doi.org/10.1007/978-1-4614-0980-9_14.
43. **Morais MC, Kanamaru S, Badasso MO, Koti JS, Owen BA, McMurray CT, Anderson DL, Rossmann MG.** 2003. Bacteriophage phi29 scaffolding protein gp7 before and after prohead assembly. Nat. Struct. Biol. **10:**572–576. http://dx.doi.org/10.1038/nsb939.
44. **Parker MH, Prevelige PE, Jr.** 1998. Electrostatic interactions drive scaffolding/coat protein binding and procapsid maturation in bacteriophage P22. Virology **250:**337–349. http://dx.doi.org/10.1006/viro.1998.9386.
45. **Kennard J, Rixon FJ, McDougall IM, Tatman JD, Preston VG.** 1995. The 25 amino acid residues at the carboxy terminus of the herpes simplex virus type 1 UL26.5 protein are required for the formation of the capsid shell around the scaffold. J. Gen. Virol. **76**(Part 7)**:**1611–1621.
46. **Cardone G, Newcomb WW, Cheng N, Wingfield PT, Trus BL, Brown JC, Steven AC.** 2012. The UL36 tegument protein of herpes simplex virus 1 has a composite binding site at the capsid vertices. J. Virol. **86:**4058–4064. http://dx.doi.org/10.1128/JVI.00012-12.
47. **Hong Z, Beaudet-Miller M, Durkin J, Zhang R, Kwong AD.** 1996. Identification of a minimal hydrophobic domain in the herpes simplex virus type 1 scaffolding protein which is required for interaction with the major capsid protein. J. Virol. **70:**533–540.
48. **Warner SC, Desai P, Person S.** 2000. Second-site mutations encoding residues 34 and 78 of the major capsid protein (VP5) of herpes simplex virus type 1 are important for overcoming a blocked maturation cleavage site of the capsid scaffold proteins. Virology **278:**217–226. http://dx.doi.org/10.1006/viro.2000.0657.
49. **Dokland T, McKenna R, Ilag LL, Bowman BR, Incardona NL, Fane BA, Rossmann MG.** 1997. Structure of a viral procapsid with molecular scaffolding. Nature **389:**308–313. http://dx.doi.org/10.1038/38537.
50. **Gordon EB, Knuff CJ, Fane BA.** 2012. Conformational switch-defective X174 internal scaffolding proteins kinetically trap assembly intermediates before procapsid formation. J. Virol. **86:**9911–9918. http://dx.doi.org/10.1128/JVI.01120-12.
51. **Gordon EB, Fane BA.** 2013. Effects of an early conformational switch defect during varphiX174 morphogenesis are belatedly manifested late in the assembly pathway. J. Virol. **87:**2518–2525. http://dx.doi.org/10.1128/JVI.02839-12.